Forecasting Neutron Star Temperatures: Predictability and Variability

Dany Page[1] and Sanjay Reddy[2]

[1]*Instituto de Astronomía, Universidad Nacional Autónoma de México, Mexico D.F. 04510, Mexico*
[2]*Institute for Nuclear Theory, University of Washington, Seattle, Washington 98195, USA*

(Received 16 July 2013; revised manuscript received 29 October 2013; published 11 December 2013)

It is now possible to model thermal relaxation of neutron stars after bouts of accretion during which the star is heated out of equilibrium by nuclear reactions in its crust. Major uncertainties in these models can be encapsulated in modest variations of a handful of control parameters that change the fiducial crustal thermal conductivity, specific heat, and heating rates. Observations of thermal relaxation constrain these parameters and allow us to predict longer term variability in terms of the neutron star core temperature. We demonstrate this explicitly by modeling ongoing thermal relaxation in the neutron star XTE J1701-462. Its future cooling, over the next 5 to 30 years, is strongly constrained and depends mostly on its core temperature, uncertainties in crust physics having essentially been pinned down by fitting to the first three years of observations.

DOI: 10.1103/PhysRevLett.111.241102 PACS numbers: 26.60.Gj, 97.60.Jd, 97.80.Jp, 98.70.Qy

Neutron star low-mass x-ray binaries (NS-LMXBs) are close binary systems in which a neutron star is accreting matter from a low-mass companion [1]. In many systems accretion is not continuous and during quiescence the neutron star surface can be observed and its temperature T_e inferred [2]. In recent years, five NS-LMXBs were observed to return to quiescence after a long period of accretion that lasted years (1.3 to 24) and have been called quasipersistent transients [3–5]. Modeling the observed evolution of T_e after accretion ends revealed that the temporal characteristics are likely set by novel processes in the outer $\sim$1 km region of the neutron star, called the crust, containing dense, solid, and superfluid matter [6–8].

During accretion, the gravitational energy released at the surface is radiated away, but nonequilibrium reactions occurring deep in the crust heat the neutron star interior. Electron capture on nuclei, pycno-nuclear (i.e., induced by pressure) fusion, and electron capture induced neutron rearrangement reactions are driven by compression during accretion [9–13]. These processes, called deep crustal heating [14], gradually heat the neutron star to a steady state temperature T_0 determined by the long term balance between accretion induced heating, and core neutrino cooling [15].

On a shorter time scale, characteristic of quasipersistent transients, heating during accretion is strong enough to drive the crust out of thermal equilibrium with the core and cooling observed immediately after should reveal the thermal relaxation of the neutron star crust [16]. Modeling two systems, KS 1731-260 and MXB 1659-29 (KS and MXB hereafter), has confirmed this expectation [6,7]. Although the crust is at high density ($\rho \simeq 10^9$–10^{14} g cm^{-3}) and novel quantum and superfluid behavior is expected, nuclear interactions are well understood at these subnuclear densities and a theoretical framework to describe the structure and thermal properties of matter exists [8,17]. Crust models are sufficiently advanced that key uncertainties associated with the thermal conductivity, heat capacity, and reaction rates needed to describe thermal relaxation have been identified and studied [18].

In this Letter, we combine a detailed model of the crust with early time cooling data from a specific source, XTE J1701-462 (XTE), to make predictions for the future evolution of its surface temperature. Our predictions can be tested in the near term and we find that further cooling is strongly correlated with its core temperature. In the long term, as additional sources entering a transient cooling phase are discovered, they will further test theoretical predictions and establish the paradigm that observed cooling is due to the thermal relaxation of the crust. In turn, this will have important consequences for the nuclear and condensed matter aspects of cold dense matter. For example, it could identify signatures of a unique phase of matter that is simultaneously solid and superfluid [8,17]. Our numerical simulations use the general relativistic code NSCOOL [19], an updated version of the code used in [15].

Evolution of temperature in the crust is determined by the heat diffusion equation (omitting GR effects for simplicity)

$$C_V \frac{\partial T}{\partial t} = \kappa \frac{\partial^2 T}{\partial r^2} + \frac{1}{r^2} \frac{\partial (r^2 \kappa)}{\partial r} \frac{\partial T}{\partial r} + Q_h - Q_\nu, \quad (1)$$

where C_V is the specific heat, κ the thermal conductivity, and Q_h and Q_ν are the nuclear heating and the neutrino cooling rates, respectively. The density and temperature dependence of C_V, κ, Q_h, and Q_ν are fairly well understood (for a recent review, see [8]) and major uncertainties can be parametrized in terms of a handful of density parameters: (i) the ion-plasma frequency $\omega_P = (4\pi Z^2 e^2 n_{\rm ion}/M^*_{\rm ion})^{1/2}$, where $n_{\rm ion}$ is the total ion density and $M^*_{\rm ion}$ is the ion effective mass and incorporates effects

due to entrainment in the inner crust [20], and Ze is the ion charge; (ii) the transition temperature T_c for neutron superfluidity in the inner crust and (iii) the impurity parameter $Q_{\rm imp} = \sum_i n_i (Z_i - \langle Z\rangle)^2/n_{\rm ion}$, where n_i is the number density of the impurity species i of charge $Z_i e$, $\langle Z\rangle e$ being the average ion charge.

Because of its high conductivity the core temperature remains nearly uniform and evolves slowly due to the high specific heat. Consequently, the thermal time scale

$$\tau_{\rm th} \sim \frac{C_V^{\rm crust}}{\kappa^{\rm crust}} (\Delta r)^2 \tag{2}$$

is set by the crust, where Δr is the crust thickness. Variations of C_V, κ, and the ratio C_V/κ are shown in the left, middle, and right panels of Fig. 1, respectively. We now briefly discuss the main sources of uncertainty for C_V and κ and their range that we will employ.

Ions form a quantum Coulomb crystal when $T < 0.1 T_P$, where $T_P = \hbar\omega_P/k_B$ is the ion plasma temperature. At these low temperatures, the ion specific heat is dominated by phonons and $C_V^{\rm ion} \propto T^3/v_t^3$, where $v_t \propto \omega_P/q_{\rm D}$ is the transverse phonon velocity and $q_{\rm D} = (6\pi^2 n_{\rm ion})^{1/3}$ the Debye momentum. v_t remains somewhat uncertain because of the coupling between dynamics of the neutron superfluid and the lattice is not known precisely [20,21]. We incorporate this uncertainty using a range of possible ion effective mass $M^*_{\rm ion}$, and hence a range of ω_P, from Am_n to $A_{\rm cell} m_n$, where $A_{\rm cell} = A + A_{\rm drip}$, A is the ion mass number, and $A_{\rm drip}$ the number of dripped neutrons in the Wigner-Seitz cell. When $\Theta_{\rm D} \lesssim T \lesssim T_m$, where T_m is the melting temperature and $\Theta_{\rm D} \sim 0.45 T_P$ the Debye temperature, $C_V^{\rm ion}$ is almost T independent and $\simeq 3k_B$, and slowly decreases in the liquid phase. The electron component is well approximated by a degenerate ultrarelativistic Fermi-Dirac gas and $C_V^e = T p_{\rm Fe}^2 (k_B^2/3\hbar^2 c)$, where $p_{\rm Fe}$ is the electron Fermi momentum. For $T \ll T_P$ electrons dominate since $C_V^e \propto T$ but with increasing T ions take over, since $C_V^{\rm ion} \propto T^3$. In the inner crust, neutrons are superfluid for $T < T_c$ and their contribution to C_V is strongly suppressed [22]. In the thin layer where $T \gtrsim T_c$ neutrons dominate C_V resulting in the C_V barrier seen in the left and right panels of Fig. 1.

Electrons dominate thermal conduction and their contribution is given by $\kappa_e = C_V^e c^2/(3\nu^e)$, where ν^e is their scattering rate. When $T \lesssim T_P$ the scattering rate is dominated by impurity scattering, even for values of the impurity parameter $Q_{\rm imp} \sim 1$. The elastic impurity scattering rate is independent of temperature and given by

$$\nu^{\rm e}_{\rm imp} = \nu^{\rm e}_0 \frac{Q_{\rm imp}}{\langle Z^2\rangle} \Lambda_{\rm imp}, \tag{3}$$

where $\nu_0^e = 4\alpha_{\rm em}^2 \langle Z^2\rangle p_{\rm Fe}/[3\pi\langle Z\rangle)]$ is the fiducial electron scattering rate in an uncorrelated gas, and $\Lambda_{\rm imp} \approx 2$ is the Coulomb logarithm for randomly distributed impurities [23].

At shallow depth explosive nuclear burning through rapid-proton captures produces an impure mix with $Q_{\rm imp} \simeq$ 30–100 [24]. However, several processes including chemical separation due to preferential freezing of large Z elements at the bottom of the ocean, and neutron-rearrangement and pycnonuclear reactions deeper in the inner crust are expected to greatly reduce $Q_{\rm imp}$ in the solid regions of the crust [11,13,25]. We treat $Q_{\rm imp}(\rho)$ as a density dependent free parameter with a value $Q_{\rm imp}^{{\rm hi}\rho}$, expected to be small at high densities, and $Q_{\rm imp}^{{\rm lo}\rho}$, possibly much higher at low densities. Modeling crust relaxation in KS and MXB has shown that $Q_{\rm imp}^{{\rm hi}\rho} \simeq$ 1–5 is necessary [7].

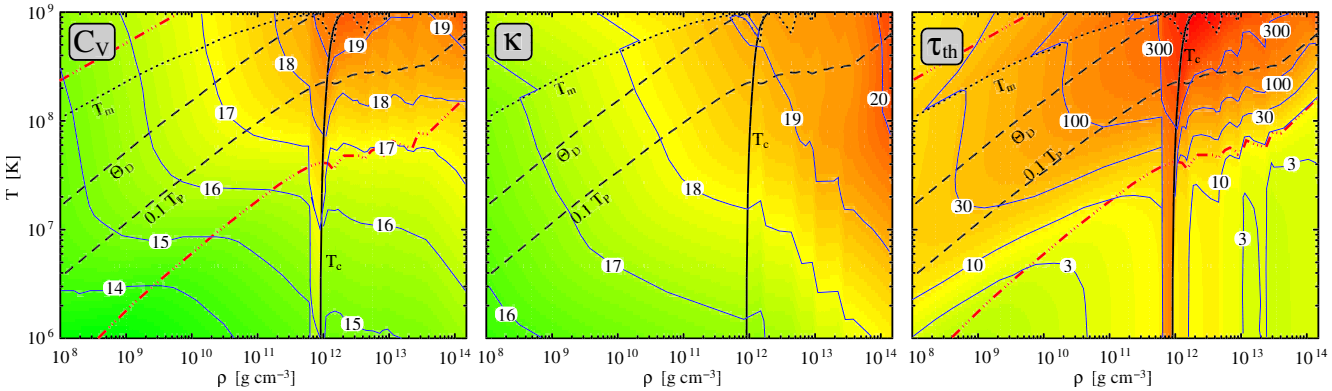

FIG. 1 (color online). The "neutron star crust landscape."Left panel: color plot of the specific heat C_V, in erg K^{-1} cm^{-3}, with (blue) contour lines labeled by $\log_{10} C_V$. Central panel: color plot of thermal conductivity κ, in erg K^{-1} cm^{-1} s^{-1}, with (blue) contour lines labeled by $\log_{10}\kappa$. Right panel: color plot of $\tau_{\rm th} = C_V/\kappa$ in time/(length)^2 with (blue) contour lines at 3, 10, 30, 100, and 300 days per (100 m)^2. In all three panels $Q_{\rm imp}^{{\rm lo}\rho} = 20$ at ρ below 10^{12} g cm^{-3} and $Q_{\rm imp}^{{\rm hi}\rho} = 4$ above 10^{13} g cm^{-3}, with a smooth transition in between. The neutron $^1S_0$ gap is from [28] which has a layer of unpaired neutrons only just above neutron drip; its T_c is shown. Also plotted on each panel is the ion melting temperature T_m [29], the Debye temperature $\Theta_{\rm D} \simeq 0.45 T_P$ [30], and $0.1 T_P$, T_P being the ion plasma temperature. In the C_V and $\tau_{\rm th}$ panels, the two (red) dash-triple dot lines mark the boundary where the ion and electron C_V are equal.

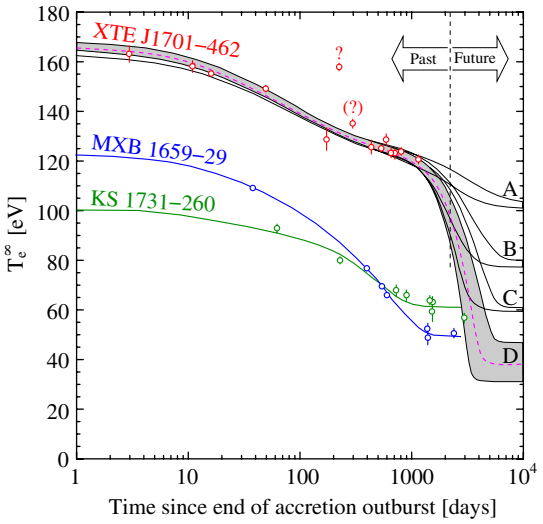

FIG. 2 (color online). Observed effective temperatures at infinity, T_e^∞ (circles with 1σ error bars), after the end of the accretion outburst of KS 1731-260 [3], MXB 1659-29 [4], and XTE J1701-462 [26]. Our theoretical models for KS and MXB, similar to those of [7], employ the crust physics displayed in Fig. 1 but with $(Q_{\rm imp}^{lo\rho}, Q_{\rm imp}^{hi\rho})$ equal to (5,3) for KS and (10,3) for MXB [31]. The dashed (magenta) curve model for XTE uses exactly the physics of Fig. 1 [31] and details are displayed in Fig. 3. The two data points marked as ? and (?) are likely and possibly, respectively, contaminated by residual accretion [26]. All our models that fit the 12 XTE data points (up to 1158 d, but excluding the two marked with ?) with a $\chi^2/12 < 1$ are shown in four bands according to the initial core temperature: *A*: $T_0 = 10^8$ K; *B*: $T_0 = 10^{7.75}$ K; *C*: $T_0 = 10^{7.5}$ K, and *D* that comprises all our models with T_0 between $10^{7.25}$ and 10^6 K. The "Past" and "Future"refer to XTE's present time. Neutron star structure is obtained using the high-density equation of state of [32] for the core and [10] for the crust, with a mass of $1.4M_\odot$ for XTE and MXB, and $1.7M_\odot$ for KS.

Deep crustal heating injects about 1.5–2 MeV of energy per accreted baryon in the density interval 10^9–10^{14} g cm^{-3} [11,12], and possibly up to 4 MeV for extreme models [13]. Since the exact accretion rate $\dot{M}$ during outburst is also uncertain, uncertainty in the injected heat is masked by varying $\dot{M}$, which is one of our model parameters. However, in all models the bulk of the heat is deposited at densities above neutron drip, and we employ the model of Ref. [12].

XTE is peculiar in that during its 1.6 yr long outburst it accreted at a high rate close to the Eddington limit, $\dot{M}_{\rm Edd} \simeq 2 \times 10^{-8} M_\odot$ yr^{-1} [26]. In contrast, accretion outbursts in MXB and KS lasted 2.5 and 12.5 yr with average $\dot{M}$ of $\sim 0.05\dot{M}_{\rm Edd}$ and $\sim 0.2\dot{M}_{\rm Edd}$, respectively [4,16]. The observed cooling light curves of these three stars are displayed in Fig. 2. XTE's evolution is characterized by a short initial cooling phase of about 100 d followed by a 2 yr long plateau. Much unlike the cooling behavior of KS and MXB which evolved on an initial time scale of $\sim$300 and $\sim$450 d followed by much slower evolution [3,27]. XTE also has, on average, a T_e^∞ twice larger than MXB and KS, implying a crust temperature about 4 times higher. XTE's evolution explores a new, hotter, regime of Fig. 1 which, together with its high $\langle \dot{M} \rangle$ and short outburst, explains its peculiar behavior as we describe below.

The left panel of Fig. 3 shows a series of temperature profiles during accretion induced heating for XTE. Heating was so strong that it would have taken several decades for XTE to reach a stationary state. In a steady state, the inverted T gradient in the crust is large enough that heat flow into the core exactly balances deep crustal heating. KS and MXB, with lower $\langle \dot{M} \rangle$, could reach a stationary state during their longer outbursts [7]. Crust microphysics in Fig. 1 naturally explains this diversity—the hotter

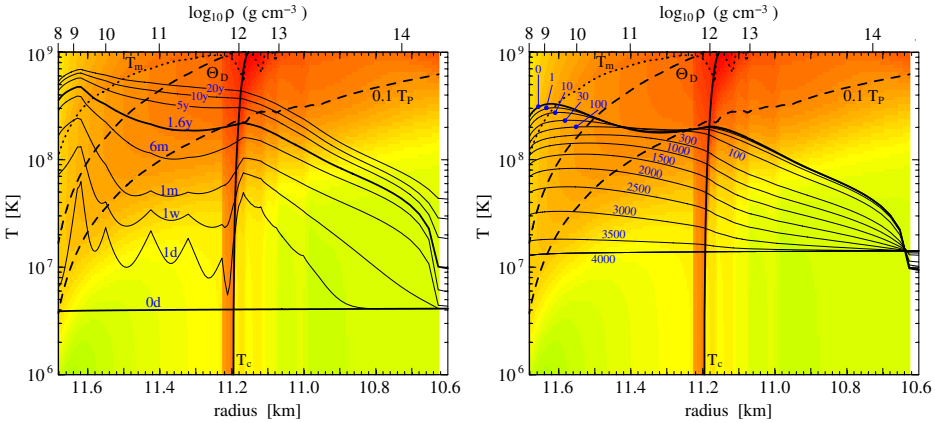

FIG. 3 (color online). Left panel: an example of the evolution of XTE's crust temperature during an accretion phase at $\dot{M} \simeq 0.9\dot{M}_{\rm Edd}$ with initial uniform $T = 4 \times 10^6$ K (labeled 0d). Profiles after 1 day (1d), 1 week (1 w), 1 and 6 months (1 m and 6 m) and 1.6 year (1.6 y) are shown. The profiles at 5, 10, and 20 years (5 y, 10 y, and 20 y) show the times needed to approach the steady state. Right panel: An example of the evolution of XTE's crust temperature profile during the cooling phase. Curves are labeled by the time, in days, from the end of the accretion outburst. In both panels the background color map is the local thermal time from Fig. 1. Notice that the core temperature is increasing both during the accretion phase and the subsequent relaxation phase.

crust in XTE (were $T \gtrsim 10^8$ K) has larger thermal time scales.

Relaxation of XTE is illustrated in the right panel of Fig. 3. The outermost, initially hot, 200 m thick layer relaxes rapidly, in about 100 d, resulting in the observed rapid initial decrease of T_e^∞. This time scale matches $\tau_{\rm th} \sim$ 30–100 d of this layer at $T \sim 2 \times 10^8$ K (see Fig. 1, right panel). Subsequent temperature evolution is slow: heat from the outer crust, whose temperature determines the observed T_e^∞, has to flow into the inner crust, and then into the core. It has to pass through the bottleneck just above neutron drip, where $\tau_{\rm th}$ is $\sim$1 yr at $T \simeq 10^8$ K, and then diffuse several hundreds of meters down to the core. This process explains the existence of a plateau in the observed T_e^∞. However, on a longer time scale, further decrease of T_e^∞ is naturally expected.

To explore how three years of observations constrain crustal properties and the future evolution of XTE we performed an extensive search of the parameter space. A synopsis of our results is displayed in Fig. 2 as four bands of cooling trajectories are labeled as "A" to "D", according to their value of T_0. A comprehensive analysis of our results will be presented in a forthcoming paper, but, in the case $T_0 < 10^8$ K, models that fit the three years of observed evolution are strongly constrained and all models in the cases B, C, and D have crust microphysics very similar to the one depicted in Fig. 1: $Q_{\rm imp}^{{\rm lo}\rho} \sim$ 15–30 and $Q_{\rm imp}^{{\rm hi}\rho} \sim$ 3–4, with a smooth shift from $Q_{\rm imp}^{{\rm lo}\rho}$ to $Q_{\rm imp}^{{\rm hi}\rho}$ at densities between 10^{12} and 10^{13} g cm^{-3}; $M_{\rm ion}^* \sim Am_n$, i.e., little entrainment; the C_V barrier due to unpaired neutrons just above the neutron drip point cannot be too strong; i.e., T_c must grow relatively rapidly at low $k_{F,n}$. (The same microphysics is also compatible with modeling of KS and MXB as shown in Fig. 2.) The dominant unconstrained parameter is the initial core temperature. In case the core is cold we also find that the crust thickness would be constrained to be $\simeq$ 1 km. The future evolution of XTE appears to be mostly determined by its previous core temperature T_0 and, for a given T_0, uncertainty in future time is smaller than a factor of 2.

It is remarkable that the crust model describes diverse cooling observed in XTE J1701-462, MXB 1659-29, and KS 1731-260 with similar input physics, and provides a natural explanation for the rapid early cooling in XTE. Its prediction for future cooling solely in terms of one unknown parameter—the core temperature—can be tested with continued monitoring of XTE. If confirmed it would firmly establish the crust relaxation as the underlying process, and taken together fits to these three sources will provide useful constraints for the thermal and transport properties of the neutron star crust. Finally, results displayed in Fig. 3 show that even the core response is not negligible, and these systems may open a new window for studying matter at even larger densities. We hope that our results will motivate a long term program to discover and monitor accreting neutron stars.

We thank Bob Rutledge for useful discussions at an early stage of this work and Andrew Steiner and Joel Fridriksson for comments on this manuscript. D. P.'s work is partially supported by grants from the UNAM-DGAPA (No. IN113211) and Conacyt (CB-2009-01, No. 132400). D. P. acknowledges the hospitality of the Theoretical Division at the Los Alamos National Laboratory, where part of this work was developed. The work of S. R. was supported by the DOE Grant No. DE-FG02-00ER41132 and by the Topical Collaboration to study neutrinos and nucleosynthesis in hot and dense matter.

[1] *Compact Stellar X-Ray Sources*, edited by W. H. G. Lewin and M. van der Klis (Cambridge University Press, Cambridge, England, 2006).
[2] R. E. Rutledge, L. Bildsten, E. F. Brown, G. G. Pavlov, and V. E. Zavlin, Astrophys. J. **514**, 945 (1999).
[3] E. M. Cackett, E. F. Brown, A. Cumming, N. Degenaar, J. M. Miller, and R. Wijnands, Astrophys. J. Lett. **722**, L137 (2010).
[4] E. M. Cackett, R. Wijnands, J. M. Miller, E. F. Brown, and N. Degenaar, Astrophys. J. Lett. **687**, L87 (2008).
[5] J. K. Fridriksson, J. Homan, R. Wijnands, M. Méndez, D. Altamirano, E. M. Cackett, E. F. Brown, T. M. Belloni, N. Degenaar, and W. H. G. Lewin, Astrophys. J. **714**, 270 (2010).
[6] P. S. Shternin, D. G. Yakovlev, P. Haensel, and A. Y. Potekhin, Mon. Not. R. Astron. Soc. **382**, L43 (2007).
[7] E. F. Brown and A. Cumming, Astrophys. J. **698**, 1020 (2009).
[8] D. Page and S. Reddy, in *Neutron Star Crust*, edited by C. A. Bertulani and J. Piekarewicz (Nova Publishing, Hauppauge, 2012).
[9] G. S. Bisnovatyi-Kogan and V. M. Chechetkin, Uspekhi Fizicheskikh Nauk **127**, 263 (1979) , Sov. Phys. Usp. **22**, 89 (1979).
[10] P. Haensel and J. L. Zdunik, Astron. Astrophys. **227**, 431 (1990).
[11] S. S. Gupta, T. Kawano, and P. Moller, Phys. Rev. Lett. **101**, 231101 (2008).
[12] P. Haensel and J. L. Zdunik, Astron. Astrophys. **480**, 459 (2008).
[13] A. W. Steiner, Phys. Rev. C **85**, 055804 (2012).
[14] E. F. Brown, L. Bildsten, and R. E. Rutledge, Astrophys. J. Lett. **504**, L95 (1998).
[15] M. Colpi, U. Geppert, D. Page, and A. Possenti, Astrophys. J. Lett. **548**, L175 (2001).
[16] R. E. Rutledge, L. Bildsten, E. F. Brown, G. G. Pavlov, V. E. Zavlin, and G. Ushomirsky, Astrophys. J. **580**, 413 (2002).
[17] C. Pethick and D. Ravenhall, Annu. Rev. Nucl. Part. Sci. **45**, 429 (1995).
[18] N. Chamel and P. Haensel, Living Rev. Relativity **11**, 10 (2008).
[19] A public version of NSCOOL is available at http://www.astroscu.unam.mx/neutrones/NSCool/.

[20] N. Chamel, D. Page, and S. Reddy, Phys. Rev. C **87**, 035803 (2013).
[21] D. Kobyakov and C. J. Pethick, Phys. Rev. C **87**, 055803 (2013).
[22] K. P. Levenfish and D. G. Yakovlev, Astronomy Reports **38**, 247 (1994).
[23] E. Flowers and N. Itoh, Astrophys. J. **206**, 218 (1976).
[24] H. Schatz, A. Aprahamian, V. Barnard, L. Bildsten, A. Cumming, M. Ouellette, T. Rauscher, F.-K. Thielemann, and M. Wiescher, Nucl. Phys. **A688**, 150 (2001).
[25] C. J. Horowitz, D. K. Berry, and E. F. Brown, Phys. Rev. E **75**, 066101 (2007).
[26] J. K. Fridriksson, J. Homan, R. Wijnands, E. M. Cackett, D. Altamirano, N. Degenaar, E. F. Brown, M. Méndez, and T. M. Belloni, Astrophys. J. **736**, 162 (2011).
[27] E. M. Cackett, E. F. Brown, A. Cumming, N. Degenaar, J. K. Fridriksson, J. Homan, J. M. Miller, and R. Wijnands, Astrophys. J. **774**, 131 (2013).
[28] A. Schwenk, B. Friman, and G. E. Brown, Nucl. Phys. **A713**, 191 (2003).
[29] W. L. Slattery, G. D. Doolen, and H. E. DeWitt, Phys. Rev. A **26**, 2255 (1982).
[30] W. J. Carr, Phys. Rev. **122**, 1437 (1961).
[31] In agreement with [7] in order to fit the early data points, we need to add an extra energy source at $\rho \sim 10^9$ g cm^{-3}. 200 and 100 keV/(accreted nucleon) are enough for KS and XTE. For MXB, however, we need to inject an extra 2 MeV/(accreted nucleon) and may indicate that the first observation was contaminated by residual accretion.
[32] A. Akmal, V. R. Pandharipande, and D. G. Ravenhall, Phys. Rev. C **58**, 1804 (1998).